**Final Report**

**Award Number:** G15AP00018

**Award Title: Calibrating Synthetic Ground Motions Damage Potential through Broadband Spectral Inversion: Collaborative Research with Colorado School of Mines, and the USGS**

**Authors:**

Peng Deng

Colorado School of Mines, 1500 Illinois St. Golden CO 80401, Phone: 303-273-3932 Fax: 303-273-3413 Email: pdeng@mymail.mines.edu

Shiling Pei

Colorado School of Mines, 1500 Illinois St. Golden CO 80401, Phone: 303-273-3932 Fax: 303-273-3413 Email: spei@mines.edu

Stephen Hartzell

US Geological Survey, Denver Federal Center, Box 25046 MS 966, Denver, CO 80225, Phone: 303-273-8572, Fax: 303-273-8600, Email: shartzell@usgs.gov

Nicolas Luco

US Geological Survey, Denver Federal Center, Box 25046 MS 966, Denver, CO 80225, Phone: 303-273-8683, Fax: 303-273-8600, Email: nluco@usgs.gov

Sanaz Rezaeian

US Geological Survey, Denver Federal Center, Box 25046 MS 966, Denver, CO 80225, Phone: 303-273-8565, Fax: 303-273-8600, Email: srezaeian@usgs.gov

Award Term: 01/15/2015~12/31/2016 (including one year no cost extension)

**Abstract**

Improve predictive relationships between strong ground shaking and damage in buildings and other structures for implementation in probabilistic hazard maps is a priority topic in research on Earthquake Effects (EE) set out in Program Announcement G14AS00036 and is the focus of this report. Specifically, this study aims to develop a calibration method for broadband synthetic ground motion models so that they will produce ground motion time series that will cause similar damage in building structures as the recorded ground motions.

Currently, validation of broadband synthetic ground motion models has been focused on comparing the mean and dispersion of ground motion characteristics such as spectral acceleration and PGA with recorded data or empirical equations. Very little work has been done to compare the effects of synthetic ground motion on building structures to that from recorded ground motions. On the other hand, with the advancement of performance based earthquake engineering (PBSE) philosophy in the engineering community, there is a strong focus on explicit modeling of structural damage and subsequent loss in modern hazard mitigation research (e.g. time history response analysis is considered as a valid design option in ASCE7). In this study, the research team intended to first develop a way to correlate ground motion spectra shape to structural damage in nonlinear systems; then apply a Broadband Spectrum Inversion (BSI) approach to "match" existing broadband models to recorded events, so that better similarity can be obtained from a building damage perspective. The success of the BSI process was validated through comparison of the actual damage generated through nonlinear time history simulation using non-linear structural models.

The work reported in this study is closely related to the effort at USGS to produce better quality ground motion models to support hazard mitigation. Through collaborative research, the deliverables from this project will be readily implementable to various applications in USGS efforts related to synthetic ground motion generation and utilization. In the long run, it is expected that the results from the study will have a positive impact on reducing losses caused by earthquakes in the United States, particularly for areas where records are scarce.

## 1. Introduction

Response spectrum is a commonly used characterization metric for ground motions (GM) in both seismological and earthquake engineering communities. By definition, response spectrum reflects the maximum acceleration or displacement responses of a linear elastic single degree of freedom (SDOF) system under a given ground motion's excitation, essentially quantifying the frequency contents of the given ground motion. In spite of some research efforts towards nonlinear response spectrum (i.e., Iwan 1980; Riddell 2008; Aydinoğlu 2003), linear response spectrum is still widely used by researchers and engineers to evaluate ground motion impact on structural systems (i.e., Loth and Baker 2015). Response spectrum does not explicitly include time domain information about the ground motions, which may be important for damage assessment in nonlinear structural systems. But it has been, to some degree, used by researchers as a key metric for evaluating the quality of synthetic motion generation, especially when seismologists want to evaluate how close their models are when compared to recorded ground motions from past events. The question this study seeks to answer is how much improvement one could obtain in regard to accurately simulating seismically induced damage in structural systems by matching synthetic ground motion response spectrum to the recorded ground motion. And if there is such benefit in match response spectrum in synthetic motion generation, what part of the response spectrum one should be focused on matching.

In structural engineering, structural response to earthquake excitation is more of a practical concern. Nowadays there is a need for (performance based seismic design) PBSD using advanced structural models, as damage is more of a concern when the design diagram is shifting towards resilience. Due to the lack of recorded data, synthetic GM were used in many studies. For example, Ellingwood et al. (2007) adopted the synthetic ground motion generated by Wen and Wu (2001) to conduct fragility assessment of concrete frames in Mid-America. The validity of the spectrum matching process is the presumption for structural analysis with synthetic GMs. However, there is still no consensus on whether this presumption holds for nonlinear structural systems. For GM with small intensity that does not cause damage (i.e. structures behave linearly), it is safe to reach the conclusion that the structural response will match closely if spectrum value at the structural natural periods are closely matched. For the GMs that are large enough to cause damage, it will still be ideal if a ground motion "damage potential indicator" (DPI) can be derived from spectra shape that can provide reasonable correlation to structural damage. But since we know linear response spectrum does not contain some information about the GM that can influence damage, to what extent this can be done (i.e. using linear spectra to derive a damage potential indicator) still remains currently obscure.

In this study, a Broadband Spectrum Inversion (BSI) approach is developed to calibrate an existing broadband model (Hartzell et al. 2005; Rezaeian et al. 2016) to recorded events. The objective of the calibration is to find key parameters in the synthetic ground motion model to produce similar damage potential to the recorded ground motion. This was done by fitting the shape of recorded response spectrum through an inversion process that was embedded in an automated program. The BSI process can be flexible in matching different regions of a response spectrum, or be programmed to optimize matching through a given functional criteria based on the shape and magnitude of the response spectrum. Some insight on how certain characteristics of the spectrum can be used for matching GM-induced structural damage between the synthetic GM and recorded GM will be needed in order to use BSI to improve damage predictability.

Because the ultimate objective of this project is to help support synthetic motion generation models to improve their "similarity" to realistic ground motions in term of structural damage, a re-constructed research question was proposed as: based on past research on DPI, can we construct a Similarity Index (SI) between two given GMs to quantify their damage potential difference? A good SI that strongly correlates with GM damage differences will in turn help us find ways to "match" GM spectrum to improve damage similarity, which are important to the broadband spectral inversion (BSI) process to improve synthetic ground motion models.

During the period of this research project, the researchers explored different ways to construct the SI based on its correlation with structural damage. After a series of trial-and-error attempts to construct an optimal SI, a critical period region for spectra shape was identified for GMs that strongly correlate with bilinear structural system damage under a given amplitude. A circular rule was defined to calculate the optimal period region in response spectrum. This will help guide synthetic ground motion generation and parameter match. Finally a group of real and synthetic ground motion were used to validate the effectiveness of the method. The research work conducted during this process, including failed attempts to generate reasonable SI, is summarized in this report for future reference.

## 2. Existing study on spectra-based damage potential indicator

This section summarizes existing studies on GM damage potential considered in this project. Note that since this project is only focused on response spectrum, other studies on damage potential relationship with non-spectrum GM characteristics (such as time domain characteristics) were not included.

The basic objective of DPI is to develop a quantitative parameter of a ground motion history that correlates strongly with the damage it will induce on a structure. In the past, many researchers have investigated various ground motion parameters that can potentially be used as DPIs. These parameters can be divided into two categories, namely structure-independent and structure-dependent DPIs. Structure-independent DPI is derived only from the ground motion itself without considering structural properties. Because structural damage is heavily influenced by structural parameters, this type of DPIs are not very robust in predicting damage. The common structure-independent DPIs can be peak values during the time history such as peak ground velocity, peak ground acceleration and peak ground displacement (Akkar and Özen 2005; Makris and Black 2004) as well as the time history-related characteristics such as Arias intensity (Arias 1970) and earthquake power index $P_a$ (Housner 1975). The compound DPIs combing the peak quantity and time history-related quantity were also used (e.g., Fajfar intensity $I_F$ (Fajfar et al. 1990), Rafael and Jaime $I_a$, $I_v$ and $I_d$ intensity to consider structural energy dissipation (Riddell and Garcia 2001), Park characteristic intensity $I_C$ (Park et al. 1985), $I_D$ index (Iervolino et al. 2006)). These structure-independent DPIs did show reasonable level of correlation with structural system responses and damage. On the other hand, most of the structure-dependent DPIs are mostly the indices derived using target structure's natural frequency information and response spectra of the GM. The mostly-used one is the 5% damped spectral acceleration ($S_a(T_1,5\%)$) at the first-mode period of a structure (i.e., Vamvatsikos and Cornell 2002; Yin and Li 2010; Bradley and Lee 2010; Ellingwood and Kinali 2009). However, when a structure vibrates into inelastic behavior, the period of the structure would be lengthened due to the fact that the structure softens under stiffness degradation (Baker and Allin Cornell 2005). In order to incorporate effect of the period elongation of the structure subjected to earthquakes, a parameter

about the response spectrum value at the lengthened period should be added in DPI to predict the nonlinear responses of interest. For example, Cordova et al. (2000) combined the spectral values at first-mode period ($T_1$) and lengthened period ($T_L$) as:

$$DPI = S_a(T_1)\left(\frac{S_a(T_L)}{S_a(T_1)}\right)^{\alpha} = S_a(T_1)^{1-\alpha} S_a(T_L)^{\alpha} \quad (1)$$

where $T_L = C \times T_1$ is the lengthened period; $C > 1$ is the coefficient about the period softening, quantifying the degree of the structure softening (namely, nonlinearity) under earthquakes. Thus, the value of $C$ should be related with intensity level of earthquakes. $\alpha$ is an undetermined coefficient to reflect spectral shape which can be seen as the weighting of the two spectral values at $T_1$ and $T_L$ (Mehanny 2009). According to the idea of constructing the DPI, Vamvatsikos and Cornell (2005) upgraded the DPI as:

$$DPI = S_a(T_s)^{1-\alpha} S_a(T_L)^{\alpha} \quad (2)$$

where the spectral value at first-mode period ($T_1$) is replaced by the one at $T_s$. The values of $T_s$ and $T_L$ can be smaller than $T_1$ to consider for the effects of high modes or larger than $T_1$ according to structural nonlinearity under earthquakes. Such definitions of $T_s$ and $T_L$ make the DPI more applicable to the tall, long-period structure dominated by higher modes of vibration or the structure controlled by strong nonlinearity under earthquake. However, these DPIs only use the information of two points in response spectrum, resulting in a lack of the information of spectral shape over a period range that the structure will transit through as it softens. In order to incorporate information of spectral shape, Bojorquez and Iervolino (2011) introduced a new DPI as:

$$DPI = \frac{1}{e}\sum_{1}^{e}\frac{S_a(T_i)}{S_a(T_1)} \quad (3)$$

Note that this DPI is dimensionless (without spectral amplitude information) and only captures the shape of the elastic response spectra. It is a spectral shape indicator between $T_1$ and $T_e$. The response spectrum in this period band is expected to exhibit an averagely positive slope for DPI>1 while negative for DPI<1. But since this particular DPI does not have the intensity information, two GMs of very different intensity can have very close DPIs as long as their shapes are similar. The limitation of these existing DPIs presents a challenge to derive reasonable similarity index (SI) between two GMs. In this project, the researchers proposed modifications to these DPIs and derived SI as the difference in DPIs between two GMs.

## 3. Response spectrum similarity index

In synthetic GM generation, it is generally believed that good synthetic models can result in similarity in response spectrum between the synthetic and real GMs. It is the hope of the researchers that these synthetic GMs will also result in similar response in structures, especially when the earthquake intensity is large and causing structural damage. For small earthquakes, this question is trivial, as matching response spectrum will result in the match of the linear maximum responses by definition. So this study focuses on one key question: What is the criteria of "good match" for response spectrum when compare synthetic and recorded GMs if the structural damage is of major concern.

One could argue that if we find a DPI that is good enough, matching that DPI will be a good starting point. It is logical except DPI itself (especially spectral value based DPI) does not map to structural damage functionally. In another word, none of the existing DPIs correspond to structural damage in a deterministic fashion. As a result, there will be a range of performance by using different DPIs to predict damage similarity. Nonetheless, DPI provided a way for us to construct a quantitative indicator that compares two response spectrum. In this study, we define a generalized Similarity Index (SI) using the difference between the DPIs of two GMs (*i* and *j*) as:

$$SI = DPI_i - DPI_j \tag{4}$$

This SI will be different based on the type of DPI used. We hypothesize that by carefully constructing DPIs, the resulted SI will show a strong correlation with structural damage similarity, which can be calculated using structural models through nonlinear time history analysis. For any given pair of GMs, one can apply them to a structure and calculate the resulting damage using time history integration, and at the same time extract an SI value based on their response spectrum. The SI and the difference in structural damage can be paired up to seek correlation. A "good" SI will be able to help maximize this correlation, and be used to guide the BSI process discussed earlier. The process of identifying suitable SI in this project is described in the following sections.

### 3.1. Subjecting reinforced concrete frames

In order to calculated real structural damage, a structural system needs to be used. Although the scope of the study will be narrowed down if structure-dependent DPIs are found later to be more effective in generating good SIs, the research team decided to pursue this direction at the beginning of the project. Initially, a three-story reinforced concrete (RC) frame was used as the target structure. The finite element of the RC frame was modelled in the previous research work in OpenSees (Mazzoni et al. 2006), making this structure a convenient choice to investigate the relationship between response spectrum similarity index and structural responses (namely, structural damages). The three bays of the frame are 6 m while the height of every story is 3 m (which is showed in Fig. 1). The cross section of the columns of the three-story frame is 500mm×500mm. For the beams of the frame, the cross section is 500mm×250mm. The column and beam are established by the 'beamWithHinges' element in OpenSees, which means the plasticity is accounted for over concentrated hinge lengths at the ends of the element (showed at Fig. 2). the length calculation of $L_{pi}$ and $L_{pj}$ depends on the length of the element, the diameter and the yield strength of the steel reinforcement within (Paulay and Priestley 1992):

$$L_p = 0.08L + 0.022 d_b f_y \tag{5}$$

where L is the length of the element; $d_b$ is the diameter of the steel bar with yield stress $f_y$.

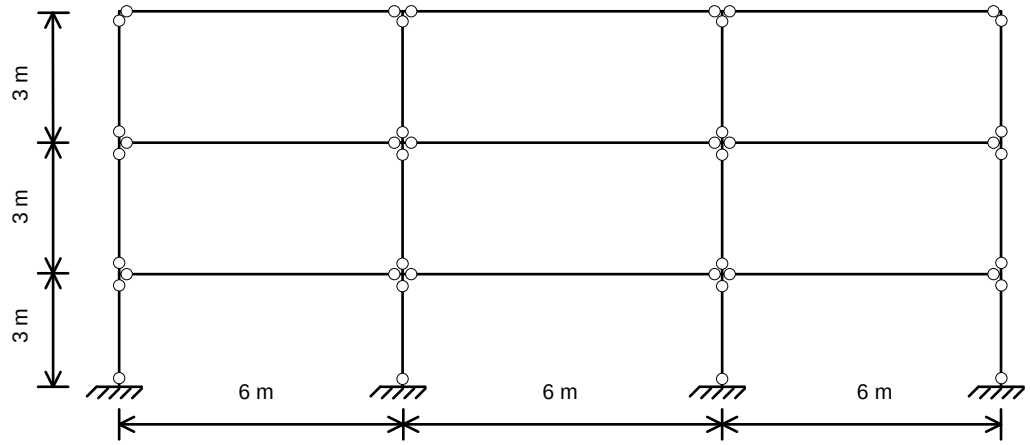


Fig. 1. Dimension of the RC frame

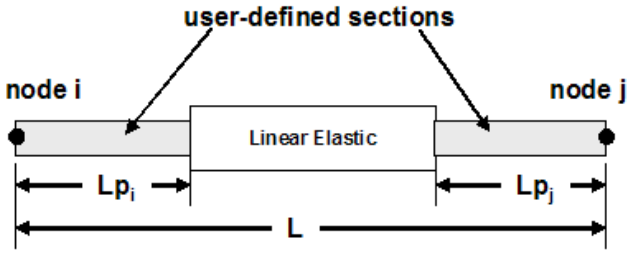


Fig. 2. 'beamWithHinges' element model.

When assessing the damage of a structure under earthquakes, researchers and engineers in the field of earthquake engineering often use maximum inter-story drift ratio because of its simple definition and strong correlated to observed damage. However, this performance indicator only considers the maximum response without taking into account the cumulative damage caused by the repeated cyclic loads (Park and Ang 1985). By combining both the maximum and cyclic loading damage mechanism, Park and Ang (1985) proposed a model called damage index both considering the member damages caused by excessive deformation and repeated cyclic loading as following:

$$D = \frac{\delta_M}{\delta_u} + \beta \frac{\int dE}{Q_y \delta_u} \tag{6}$$

where $\delta_M$ indicates the maximum deformation under earthquake; $\delta_u$ and $Q_y$ are the calculated ultimate deformation and yield strength under monotonic loading, respectively (Calvi et al. 2003);

$\int dE$ is the absorbed hysteretic energy which can be obtained through the rotation of plastic hinges

of an element. Note that the damage index above is focused on the damage of members (i.e. a component level damage index). The damage to a building will be affected by the distribution of damaged members within the building (Park et al. 1985). Thus, the overall damage index $D_T$ of the entire structure (used in the following analysis) was calculated as the weighted sum of the all member damage indices. The weighted factor $\lambda_i$ is calculated by the ratio of the energies absorbed by the $i^{th}$ member and the total energy dissipation:

$$D_T = \sum_i \lambda_i D_i \tag{7}$$

$$\lambda_i = \frac{E_i}{\sum E_i} \tag{8}$$

In order to compare the differences of $DI_i$ and $DI_j$ of the frame building brought by $i^{th}$ and $j^{th}$ ground motions (corresponding to the ground motion response spectrum similarity index), the formula to describe the differences is introduced:

$$\Delta DI = DI_i - DI_j \tag{9}$$

Fig. 3 shows the time history drift ratios of the RC frame under two different ground motions (both from Northridge Earthquake, “cpp” and “jfp” are the station ID and the corresponding information is listed in Table 1). The DI under a ground motion is calculated through the maximum drift ratio and the cumulative damage. The value of DI is positively related with maximum drift ratio but the relation is not constant because the cumulative energy dissipation is also consider in DI calculation.

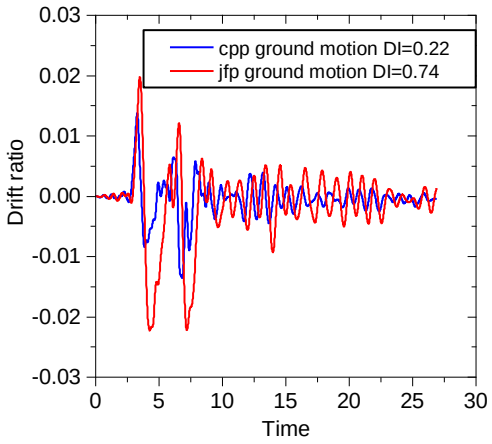


Fig. 3. Example of time history drift ratio of the RC frame

### 3.2. Spectral amplitude SI to predict ΔDI of the RC frames

With the difference in DI (ΔDI) calculated following the procedure described in section 3.1, the research team started to try different SI formulations by using different DPI formulas. The ultimate objective is to identify strong correlation with the ΔDI. Firstly, similarity index based on spectrum amplitude was explored. Three SIs derived from spectral amplitude were investigated. Because the discussion was framed with the intension to use these SIs to guide synthetic GM generation, the SIs are calculated between a recorded GM and its synthetic counterpart.

$$SI_{amp1} = \frac{1}{n}\sum_{i=1}^{n}\left[\frac{S_a^x(t_i) - S_a^y(t_i)}{S_a^y(t_i)}\right] \tag{10}$$

$$SI_{amp2} = \frac{1}{n}\sum_{i=1}^{n}\left[S_a^x(t_i) - S_a^y(t_i)\right] \tag{11}$$

$$SI_{amp3} = S_a^x(T_1)\left(\frac{S_a^x(t)}{S_a^x(T_1)}\right)^{0.5} - S_a^y(T_1)\left(\frac{S_a^y(t)}{S_a^y(T_1)}\right)^{0.5} \tag{12}$$

where the $S_a^x(t_i)$ means the spectral acceleration value at period $t_i$ for one of the 88 ground motions while $S_a^y(t_i)$ indicates the spectral value of one of the remaining of 87 ground motions (unit is g); $T_1$ indicates the first mode period of the structure. $t$ is the period needed to be determined. The number of $n$ depends on the period bands elected and the period interval. The $SI_{amp1}$ is the normalized difference of two ground motions in terms of spectral acceleration among a period range. The $SI_{amp2}$ is a variation of $SI_{amp1}$ without normalization. $SI_{amp3}$ only considers two points in their spectra at first-mode period $T_1$ and the other period longer or smaller than $T_1$. These three amplitude similarity indices take the amplitude difference at a series of periods into account. The responses of a structure can be affected by its higher modes

(primarily before damage occurs) and nonlinear yielding behavior, which essentially lengthens its effective period as structure yields. This is the main consideration when the SI includes more spectra values than just at $T_1$. Apparently, the period ranges in the three amplitude similarity indices can include the periods smaller than $T_1$ to account for higher mode effects.

In order to assess the effectiveness of the proposed SIs, a pool of GMs needs to be used so that multiple SI and ΔDI pairs can be generated. At this point, the source of the GMs actually does not matter, because the SI should perform (show strong correlation with ΔDI ) for any arbitrary GM pairs. The research team has previously generated three groups of synthetic GMs for a pool of 22 recorded GMs from Northridge (shown in Table 1). Thus this mixed pool of 88 GMs were used in this study as the "testing GM suite". Within this suite, one can derive the 3828 pairs of GMs for generating SI and ΔDI through random combination (88×87/2=3828). Once the 88 GMs were applied to the concrete frame through NLTHA using OpenSees, the 3828 sets of ΔDI can be readily calculated from model responses. But the calculation of SIs will depend on the period range that defines the SIs. The research team conducted extensive sensitivity analysis and identified the period range for each SI that maximized the SI- ΔDI correlation (assessed by the coefficient of determination, $R^2$). The resulting strongest correlation plots are shown in Fig.4 with the period range parameters given.

From Fig.4, one can learn that $SI_{amp2}$ have larger $R^2$ against structural responses ΔDI, compared with other two SIs. But $SI_{amp2}$ still has a very large scatter to be qualified as a good predictor. For example, when $SI_{amp2}$=0, the value of ΔDI of the RC frame varies between about -0.5 and 0.5. This indicates that even if we use BSI to reduce SI to 0, the damage similarity still cannot be guaranteed with reasonable accuracy. In another word, the "slope" of the correlation plot shown in Fig.4(b) is too high. Additionally, the period range parameters identified here are very likely related to the structural properties of the concrete frame used. From this point, the research can be conducted in two different directions. First one is to accept the level of scatter embedded in $SI_{amp2}$, and start to conduct sensitivity analysis of how the optimal period range will be affected by structural parameters. The second one is to seek additional ways to reduce the level of scatter first. The research team understood that the predictability of damage similarity using response spectrum similarity (i.e SI) has a limit, because response spectrum does not reflect time domain information of the earthquake that may be important to damage. However, the team also wanted to dig deeper to identify the full-potential of the SI predictability. With this intention in mind, after several meetings, the team assumed that SI formulation with only the amplitude component of the spectrum is not enough. Matching response spectrum in terms of amplitude (or average amplitude over a period range) does not mean that the segments of the response spectra overlap. Fig. 5 shows the different shape (or slope) of two ground motions but with $SI_{amp2}$=0. It was assumed that the situation showed in Fig.5 is a main reason of the large scatter of amplitude similarity index (e.g., ΔDI is between -0.5 and 0.5 for the case $SI_{amp2}$=0 in Fig. 4). Thus, the research team took the second pathway to pursue better predictability in SIs through introduction of the spectral slope in SI formulation.

Table 1 Information of 11 Northridge stations

| No. | Station Code | Location Name | Latitude | Longitude | Site Category |
|---|---|---|---|---|---|
| 1 | cpp | Canoga Park # 53 | 34.212 | -118.605 | D |
| 2 | hol | Van Nuys Hotel | 34.221 | -118.471 | D |
| 3 | jem | Jensen Filter Plant Generator Building | 34.313 | -118.498 | C |
| 4 | jfp | Jensen Filter Plant Administration Bl. | 34.312 | -118.496 | C |

| | | | | | |
|---|---|---|---|---|---|
| 5 | nwp | Newhall | 34.388 | -118.533 | D |
| 6 | par | Pardee | 34.435 | -118.582 | D |
| 7 | rrs | Rinaldi Receiving Stan-FF | 34.281 | -118.479 | D |
| 8 | sfp | Arleta | 34.237 | -118.439 | D |
| 9 | syf | Sylmar County Hospital | 34.326 | -118.444 | CD |
| 10 | van | Sepulveda VA Hospital | 34.249 | -118.478 | D |
| 11 | wc1 | White Oak Church # 003 | 34.209 | -118.517 | D |

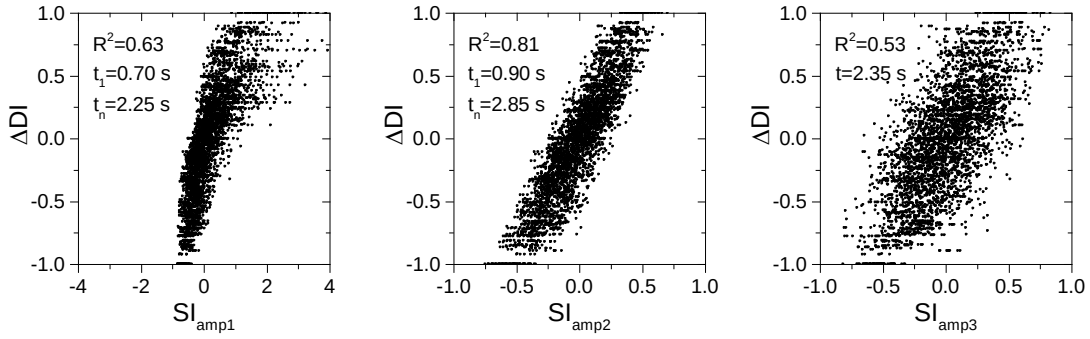


(a) (b) (c)

Fig. 4. Correlation relationship between ΔDI of the RC frame and (a) $SI_{amp1}$, (b) $SI_{amp2}$ and (c) $SI_{amp3}$

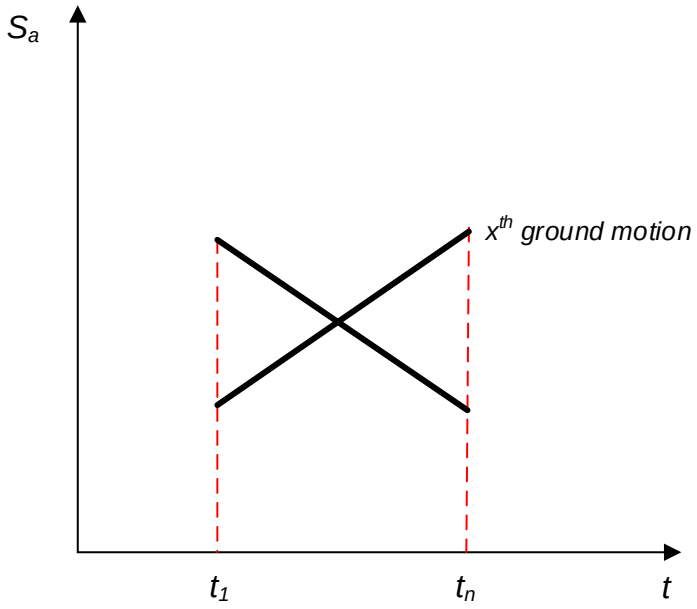


Fig. 5. Different shape of the $x^{th}$ and $y^{th}$ ground motion response spectrum with $SI_{amp2}$=0 .

### 3.3. Introducing spectral shape to reduce the prediction scatter of the amplitude-only SI

In order to effectively present the spectrum similarity of ground motions, three SIs about the spectral slope difference of ground motions among certain period range were introduced as following:

$$SI_{slo1} = \frac{\sum_{i=1}^{n}\left(t_i - \bar{t}\right)\left(\varepsilon\left(t_i\right) - \bar{\varepsilon}\right)}{\sum_{i=1}^{n}\left(t_i - \bar{t}\right)^2},\ \varepsilon\left(t_i\right) = S_a^x\left(t_i\right) - S_a^y\left(t_i\right),\ \bar{\varepsilon} = \frac{1}{n}\sum_{i=1}^{n}\varepsilon\left(t_t\right) \tag{13}$$

$$SI_{slo2} = \sum_{i=1}^{n}\frac{S_a^x\left(t_i\right) - S_a^x\left(t_1\right)}{\left(t_i - t_1\right)} - \sum_{i=1}^{n}\frac{S_a^y\left(t_i\right) - S_a^y\left(t_1\right)}{\left(t_i - t_1\right)} \tag{14}$$

$$SI_{slo3} = \sum_{i=1}^{n}\frac{S_a^x\left(t_{i+1}\right) - S_a^x\left(t_i\right)}{\left(t_{i+1} - t_i\right)} - \sum_{i=1}^{n}\frac{S_a^y\left(t_{i+1}\right) - S_a^y\left(t_i\right)}{\left(t_{i+1} - t_i\right)} \tag{15}$$

where $\bar{t}$ is the mean value of the selected period band; $t_1$ is the starting period identified in amplitude SI. So, $SI_{slo1}$ represents the slope difference between record and synthetic spectrum across a given period range. $SI_{slo2}$ is the sum of tangent slope differences with respect to a specific starting period point. $SI_{slo3}$ is the sum of the tangent slope differences with respect to each segment in a specific period range (showed in Fig. 6). When the slope similarity index approaches zero, the slopes of the ground motions will match closely. These slope SIs do not account for the relative amplitude comparison. If only slope SI is used regardless of amplitude SI, a segment of the spectra for a certain period band might be parallel ($SI_{slo}$=0) while the amplitude of the spectrum are very different (showed as Fig. 7). It is apparent that the amplitude SI and slope SI should be applied together in order to accurately predict structural damage by ground motion response spectrum. So in this study, the slope SI is considered for cases (pairs) where the amplitude SI is zero. The hypothesis is that by adding the slope information, the predictability of the SIs should improve when original amplitude SI cannot help to differentiate different cases.

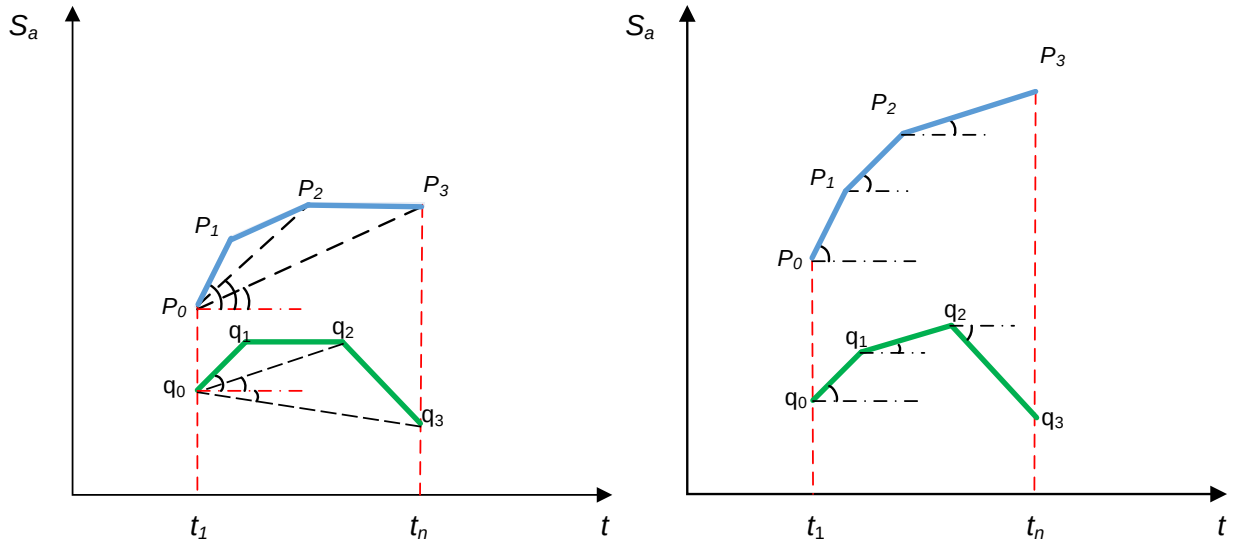


Fig. 6. Illustration of $SI_{slo2}$ and $SI_{slo3}$.

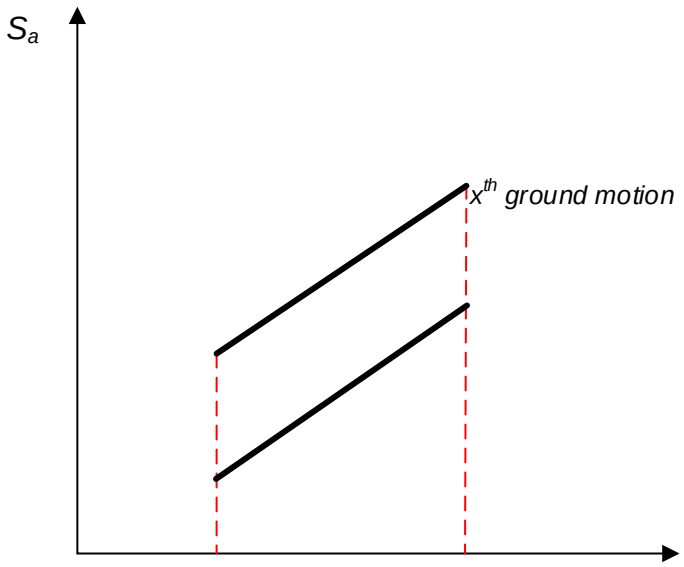


Fig. 7. A segment of the two parallel response spectra with zero slope SI.

Because former analysis has shown that $SI_{amp2}$ has a very strong correlation with ΔDI ($R^2$=0.81), it was adopted as amplitude SI. From Fig. 4(b), one can learn that the scatter of ΔDI is large when $SI_{amp2}$ is close to zero. The data points with $SI_{amp2}$ close to zero (i.e. GM pairs that produced 0 amplitude SI) were selected as a sub-group to investigate whether or not the slope SIs can help to reduce the scatter. Fig. 8 illustrates the correlation between ΔDI and there slope similarity indices when $SI_{amp2}$ is close to zero. If the slope SIs can bring new level of insight into the process and add predictability, a correlation pattern should emerge. This analysis is simpler than the analysis conducted for amplitude SI because now the period range is given (from past analysis). It is logical for the amplitude and slope SIs to use the same period range. If it is found out that one of the slope SIs can help improve predictability, another sensitivity analysis can be conducted to optimize the period range between slope and amplitude SIs. However, from the data presented in Fig.8, the three slope SIs are all ineffective in providing useful information to reduce the scatter of selected amplitude SI.

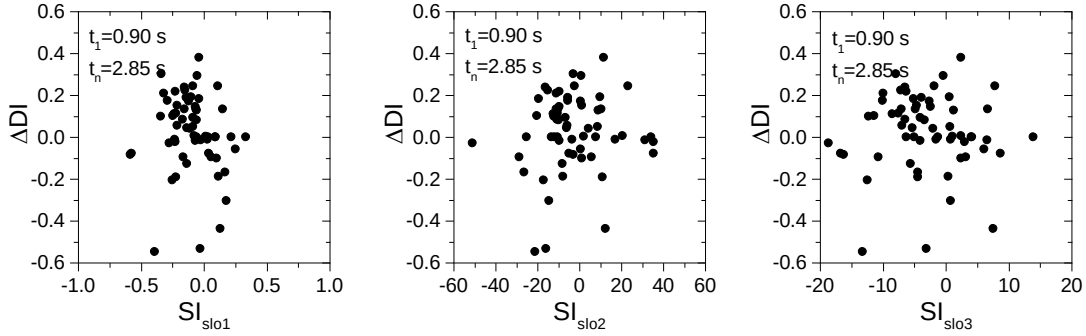


(a) (b) (c)

Fig. 8. Correlation between ΔDI and (a) $SI_{slo1}$, (b) $SI_{slo2}$ and (c) $SI_{slo3}$.

### 3.4. Summary of amplitude and slope SIs

Three different amplitude SIs were investigated to find out the strongest possible correlation and predictability with respect to RC frame damage. The results show that the $SI_{amp2}$

present better correlation relative to another two amplitude SIs. However, even though $SI_{amp2}$ can capture the general trend in damage similarity, it still has large scatter in the structural damage prediction. In order to reduce the prediction scatter, three slope SIs were introduced to investigate whether they can provide extra information about damage similarity, but the result was negative. The three slope SIs cannot decrease the dispersion for amplitude SI.

## 4. Similarity index vector for SDOF bilinear systems

Through discussions within the research team, it was realized that the RC frame used in the first half of the project may be too specific for the purpose of identifying a useful SI. As it is clear from the investigation so far that the SI will be structure-dependent, using simpler but more generalized nonlinear systems such as a single-degree-of-freedom (SDOF) bilinear oscillator will help reduce the complexity on the structure side. This will also help simplify the damage calculation, as the ductility of the bilinear system is a simple but widely accepted damage indicator. Additionally, learning from the investigation of amplitude and slope SIs, it was decided that both the amplitude and slope information should be included when comparing two GMs. But it is difficult to combine these two types of similarity indicator algebraically, thus a similarity index consisting of two components, i.e. a vector DPI (including components representing the spectral amplitude and shape similarity separately) was introduced to investigate its correlation with the ductility of SDOF bilinear systems.

### 4.1. Bilinear SDOF systems

A bilinear SDOF systems without strength degradation is one of the simplest nonlinear systems that can be related with more complicated structures. It can be defined through four parameters: the initial elastic period ($T_1$), the damping ratio ($\xi$), the hardening ratio ($\alpha$, defined as the post-yielding stiffness divided by the initial stiffness) and a yield displacement coefficient ($C_y$). $C_y$ is a normalized parameter related with the yield displacement and elastic period (Deng et al. 2017):

$$C_y = \frac{d_y}{mg / k_1} \tag{16}$$

where $d_y$ is the yield displacement; $m$ is the mass; $k_1$ is the elastic stiffness; $g$ is the gravity acceleration. The hysteretic model of SDOF bilinear system can be seen in Fig.9.

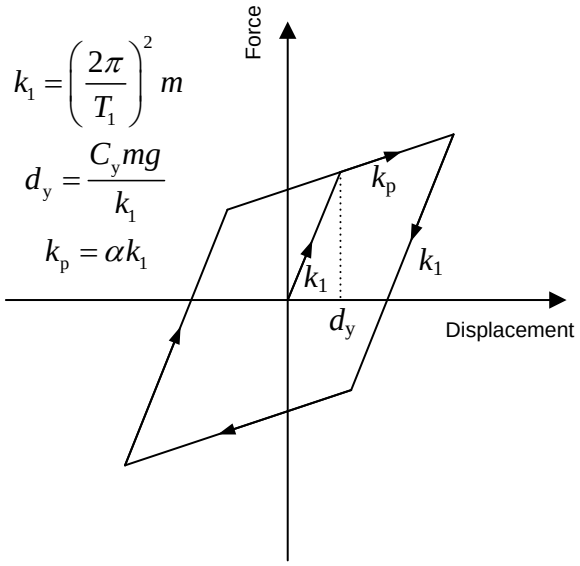


Fig. 9. Hysteretic model of the bilinear SDOF system

### 4.2. DPI vector

In order to increase its robustness, a DPI should include both the spectral amplitude and spectral shape information. Baker and Cornell (2005; 2006) proposed a vector-valued DPI consisting of spectral acceleration and epsilon to predict structural seismic performance. Although both the spectral magnitude and spectral shape are reflected in this DPI, the spectral shape information is very limited since only the shape information at one point is included. Herein, a spectral shape parameter is proposed to be similar as Eq. (17). It is starting at $T_s$ instead of $T_1$, which can allow the shape parameter to be involved in the effects of higher mode and nonlinearity. Thus, the proposed spectral shape parameter can be formulated as:

$$p_1 = \frac{1}{e-s}\sum_{s}^{e}\frac{S_a(T_i)}{S_a(T_1)} \tag{17}$$

It is evident that $p_1$ includes the spectral shape information in the period range from the starting period $T_s$ and the ending period $T_e$. $s$ means the point number at starting period while $e$ indicates the point number at ending period. Apparently, this DPI component does not include information about GM intensity. But it is expected that the optimal period range will be dependent on GM intensity. To better quantify the interplay between structural nonlinearity and seismic intensity, the indicator $\lambda$ was formulated to reflect intensity information by normalizing the spectrum value at the system fundamental period to the yielding intensity:

$$\lambda = \frac{I}{S_{a0}(T_1)} = \frac{S_a(T_1)}{S_{a0}(T_1)} \tag{18}$$

where $S_{a0}(T_1)$ indicates the spectral acceleration at which the ground motion starts to yield the structure. When $\lambda \leq 1$, the structure remains linear elastic during the GM excitation. The structure will only experience damage if $\lambda > 1$. This parameter was used as the 2nd component of the DPI vector as:

$$DPI = [p_1, p_2] = \left[ \frac{1}{e-s} \sum_{s}^{e} \frac{S_a(T_i)}{S_a(T_1)},\ \lambda \right] \tag{19}$$

If we use this DPI vector to describe GM spectrum, it can be hypothesized that when the two ground motions match well at $p_1$ and $p_2$, the damage of the structure (can be represented by ductility of the bilinear system) caused by the two ground motions will be similar. The DPI vector proposed here is apparently structure-dependent. Firstly the intensity component is defined at the natural frequency of the structure, as well as the yielding intensity (in case of bilinear system, it is actually equal to the parameter Cy introduced earlier).

$$S_{a0}(T_1) = d_y \omega_n^2 / g = C_y \tag{20}$$

Secondly, the start and end period values to calculate the shape component is related to structural system parameters. Applying this to comparison of two GMs, we hypothesize that for a given bilinear system, there is an underling rule to construct the DPI vector so that good correlation between ΔDPI and damage difference can be achieved. This hypothesis was investigated in the following sections.

### 4.3. Earthquake ground motion suite

In order to find the general rule for constructing DPI vector to obtain optimal damage correlation, a suite of earthquake GMs should be applied to various bilinear systems. Recall at the beginning of this study, a GM suite of 88 motions was used including recorded and synthetic GMs. One concern of the research team was that these GMs are all from one earthquake event (Northridge) and thus not general. In order to study the new DPI vector, another set of 102 far-fault earthquake records selected from FEMA P695 (FEMA-P695 2009) project and an existing literature (Medina and Krawinkler 2004) was used. They are all recorded GM from earthquake events from 5.8M to 7.6M and different fault mechanisms such as reverse and strike-slip. The response spectra spectrum of the selected 102 ground motions are shown in Fig. 10(a).

Because the DPI vector has two components, the evaluation of the SI becomes complicated. Certainly if both DPI components are close, we can conclude that the two GMs are very similar. Consider the situation where the intensity components ($\lambda$) of the GMs are close, but the shape components are different, or verse visa, it is difficult to quantify the SI. One way to accomplish this is to add constrain to one of the DPI components when comparing two GMs. For example, instead of comparing two GMs that have different intensity and shape component, one can scale both GMs to have the same intensity component and study the relationship between the shape component similarity and damage similarity calculated from time history simulation. Putting this in the context of synthetic GM generation and BSI, it indicates that to better match damage potential of a recorded GM, the procedure should match the intensity component first,

and then match the shape over a given period range as close as possible. Fig. 10(b) showed an example of adding this intensity constrain to the new 102 GM suite, assuming the natural period of the structural system is at 0.5 sec.

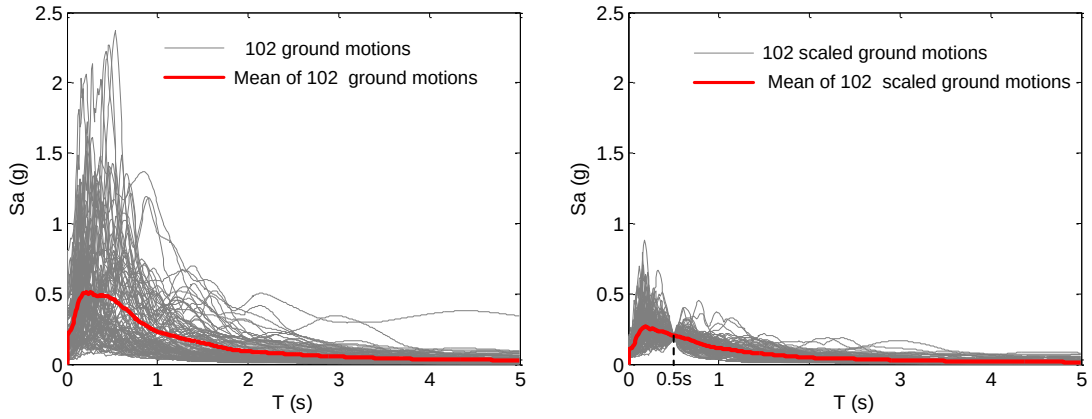


(a) (b)

Fig. 10. 5% damped response spectra of (a) original ground motions and (b) scaled ground motions

### 4.4. Maximizing damage correlations for SDOF bilinear systems

#### 4.4.1. Circle rule of optimal period range

Following a similar process as before, the optimal period range for the shape DPI component is sought using data generated from the GM suite described above. Note that this was done for different intensity levels by scaling the GM suite to different $\lambda$ values. The coefficient of determination ($R^2$) was adopted to describe how well a linear relationship is fitted between the shape DPI difference and the ductility (damage) difference. Because the rule will also depend on structural parameters, different bilinear SDOF systems with $\xi$=5%, $\alpha$=0.2, $C_y$=0.2 and $T_1$=0.5s, 1.0s, 1.5s were selected to investigate the correlation trends. The 102 ground motions can construct 5151 sets of two ground motions and thus produce 5151 comparative pairs of GMs. The value of $R^2$ were obtained through the correlation analysis between these 5151 data points for different structural parameter, value of $\lambda$, and a varying period range [$T_s$, $T_e$]. Fig. 11 shows the contour plots of $R^2$ for different situations against a $T_s$-$T_e$ space, in which one point represent a unique starting periods and ending periods range as long as the point is above the $T_s$=$T_e$ line. From the contours, it can be observed that by change the value of [$T_s$, $T_e$] (moving the point within the $T_s$-$T_e$ space), there exists an area in the $T_s$-$T_e$ plot where $R^2$ is maximized. This period range is considered as the optimal range for the given structural parameters and $\lambda$ value (intensity). It should be noted that there is a fairly large region on the $T_s$-$T_e$ plot that $R^2$ is generally very close to the maximum value (with negligible, i.e., < 0.1, difference). Therefore instead of locating the absolute maximum correlation, any point period band in this area can be regarded as a satisfactory period range for constructing the DPI shape component. Based on this observation, the researchers started to look for trends in the location of this optimal region as the value of $\lambda$ and structural parameters change.

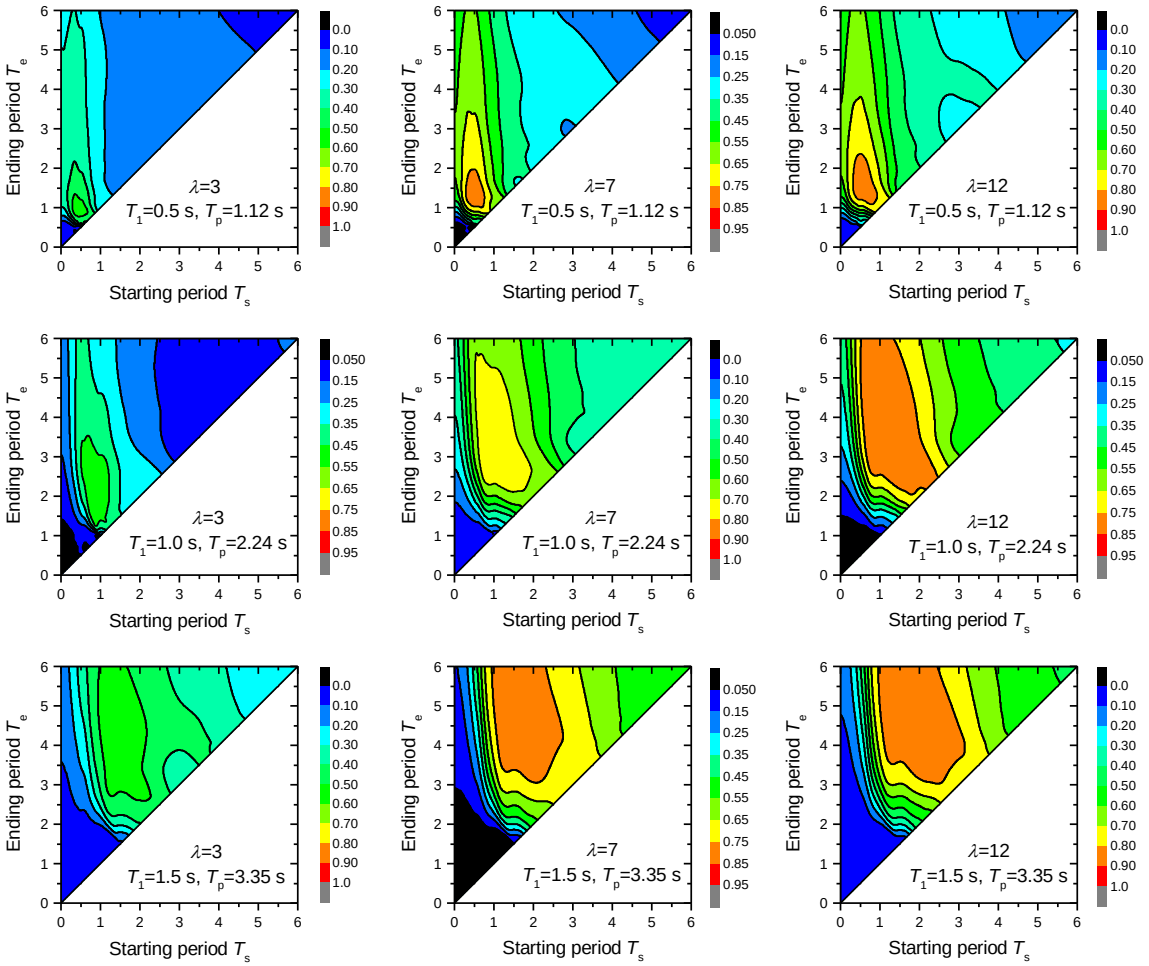


Fig. 11. $R^2$ contour results for the bilinear SDOF system with $T_1$=0.5 s, 1.0 s and 1.5 s.

In Fig. 11, one can see that the area with the largest $R^2$ is moving up towards to the point [$T_p$, $T_p$] as intensity level $\lambda$ is increased for a given system with $T_1$. It indicates that the response of the bilinear SDOF system becomes increasingly dominated by its post-yield stiffness ($k_p$) as the intensity level gradually increases. In the area with the largest $R^2$, a point closer to the diagonal line indicates a narrower period range. For BSI or other engineering applications, a narrower period range is more preferable as the need for response spectrum matching can be reduced. These points are selected and shown in Fig. 12. It can be observed that the distribution of these points roughly follow the curve of a circle which has the origin [$T_p$, $T_1$] and the radius $T_p$-$T_1$. These points also move towards [$T_p$, $T_p$] when the intensity level $\lambda$ gradually increases. Therefore, it is proposed that the optimal period range for bilinear system follows a "circle rule" on the $T_s$-$T_e$ plot. The location of the optimal period range can be found on the circle, with its location dictated by the intensity level $\lambda$. If $\lambda$=1, the system behaves as linear elastic and the optimal period band point locates at the start points of the circle ($T_1$, $T_1$), which is expected since the linear system response can be perfectly matched using just one point on the spectrum. As $\lambda$ increases, the system response is increasingly dominated by the nonlinear response and the optimal period band point gradually approaches the end point of the circle ($T_p$, $T_p$). The circle can trace the variation of the optimal period band points with different intensity levels $\lambda$, and this

phenomena is defined herein as the circle rule. This circle rule can be mathematically formulated as:

$$\left(T_s - T_p\right)^2 + \left(T_e - T_1\right)^2 = \left(T_p - T_1\right)^2 \quad T_1 \le T_s, T_e \le T_p \tag{21}$$

$$T_p = \alpha^{-0.5} T_1 \tag{22}$$

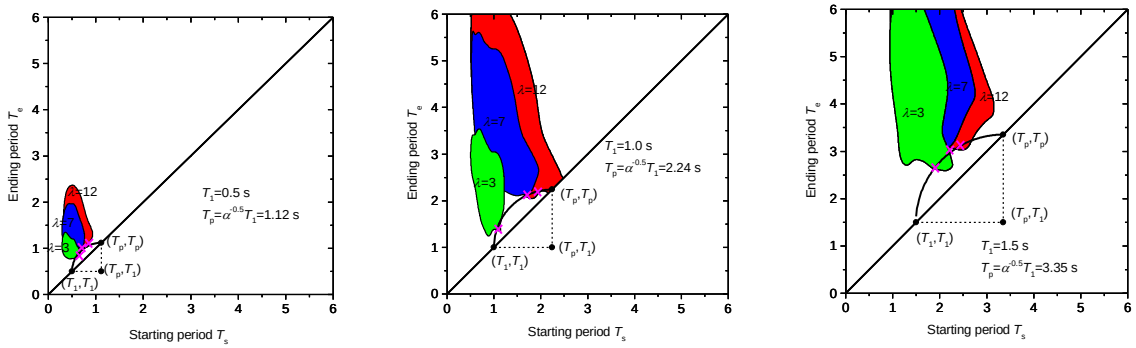


Fig. 12. Illustration of circle rule of optimal period band

### 4.4.2. Influence of λ on optimal period band

Given the circle rule mentioned above, the relation between the $\lambda$ and the location of optimal period range point on the circle is sought through regression analysis. As discussed above, the optimal period range point is moving along with the circle curve from the point [$T_1$, $T_1$] to [$T_p$, $T_p$] with the intensity level $\lambda$ increasing. Once the starting period $T_s$ is determined, the ending period $T_e$ of the optimal range can be calculated according to Eq. (21). According to the proposed circle rule and basic structural dynamic, the extreme cases for the relationship between $T_s$ and $\lambda$ can be expressed as:

$$T_s = T_1 \quad for\ \lambda = 1 \tag{23}$$

$$T_s \to T_p \quad for \lambda \to \text{infinite} \tag{24}$$

Considering the constraints of the two extreme cases, the relationship between $T_s$ and $\lambda$ can be formulated as:

$$T_s = T_p - \left(T_p - T_1\right)\beta^{\lambda - 1} \tag{25}$$

where $\beta$ is a variable smaller than 1 and assumed to be related with structural parameters $T_1$, $\alpha$ and $C_y$. Damping ratio is considered as 5% in this study.

When $T_1$ and $\alpha$ remain unchanged, $C_y$ is positively proportional to the displacement demands for a given intensity level $\lambda$ as following (Deng et al. 2017):

$$\frac{D_2}{C_{y2}} = \frac{D_1}{C_{y1}} \tag{26}$$

where $D_2$ is the displacement demand for the system with $C_{y2}$ while $D_1$ is the displacement demand for the system with $C_{y1}$ for a given intensity level $\lambda$. Since $C_y$ is positively proportional to yield displacement with other structural parameters unchanged (Eq. (16)), Eq. (26) implies that the ductility demands are independent of $C_y$. Thus one can learn that the structural parameter $C_y$ will not affect the value of $R^2$ when doing the damage correlation analysis as well as the variable $\beta$ in Eq. (25). In order to validate the conclusion about $C_y$, contours of $R^2$ with different period bands for different bilinear SDOF systems ($\alpha$=0.2, $\xi$=5%, $T_1$=0.5s, and $C_y$=0.1, 0.2, 0.3) are showed in Fig. 13, which illustrates that the contours of $R^2$ remain unchanged for different $C_y$ values.

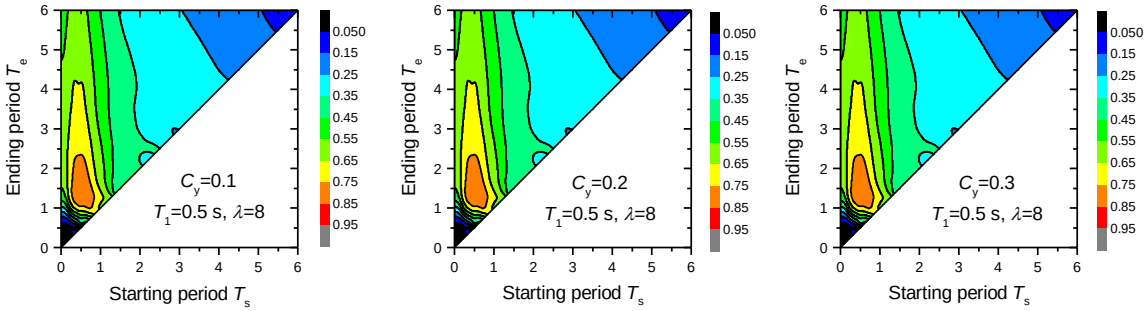


Fig. 13 Contours of $R^2$ for bilinear systems with $C_y$=0.1, 0.2, 0.3.

Through the analysis above, one can eliminate the dependence of $\beta$ to $C_y$ and can now focus on remaining structural parameters $T_1$, and $\alpha$. In order to investigate how the value of $\beta$ is related with $T_1$, and $\alpha$, the 5% damped SDOF bilinear systems with $T_1$=0.5 s, 1.0 s and 1.5 s, and $\alpha$=0.05, 0.1, 0.2 are selected. Fig. 14 illustrates that all the SDOF bilinear systems with different intensity levels are fit by to the circle rule. The colored areas for each case present the largest $R^2$ under intensity level $\lambda$=3, 4…13. Through selecting the intersection points of the areas and the circle, a regression analysis about Eq. (25) was conducted to determine the relationship between $\lambda$ and the optimal starting period (showed in Fig. 15). Fig. 15 illustrated that the effects brought by the difference of structural parameters will be enlarged with increasing intensity level $\lambda$. For the systems with short natural periods such as $T_1$=0.5s, the influence of hardening ratio on the relationship can be ignored under intensity level $\lambda$<15. Additionally, the value of $\beta$ is proportional of the hardening ratio $\alpha$ (e.g., negatively proportional for the system with $T_1$=0.5 s, but positively proportional for the systems with $T_1$=1.0 s and 1.5 s). As to the systems with different values of structural parameters, a linear interpolation can be adopted to compare the response demands caused by different ground motions such as record ground motion and the corresponding synthetic ground motion.

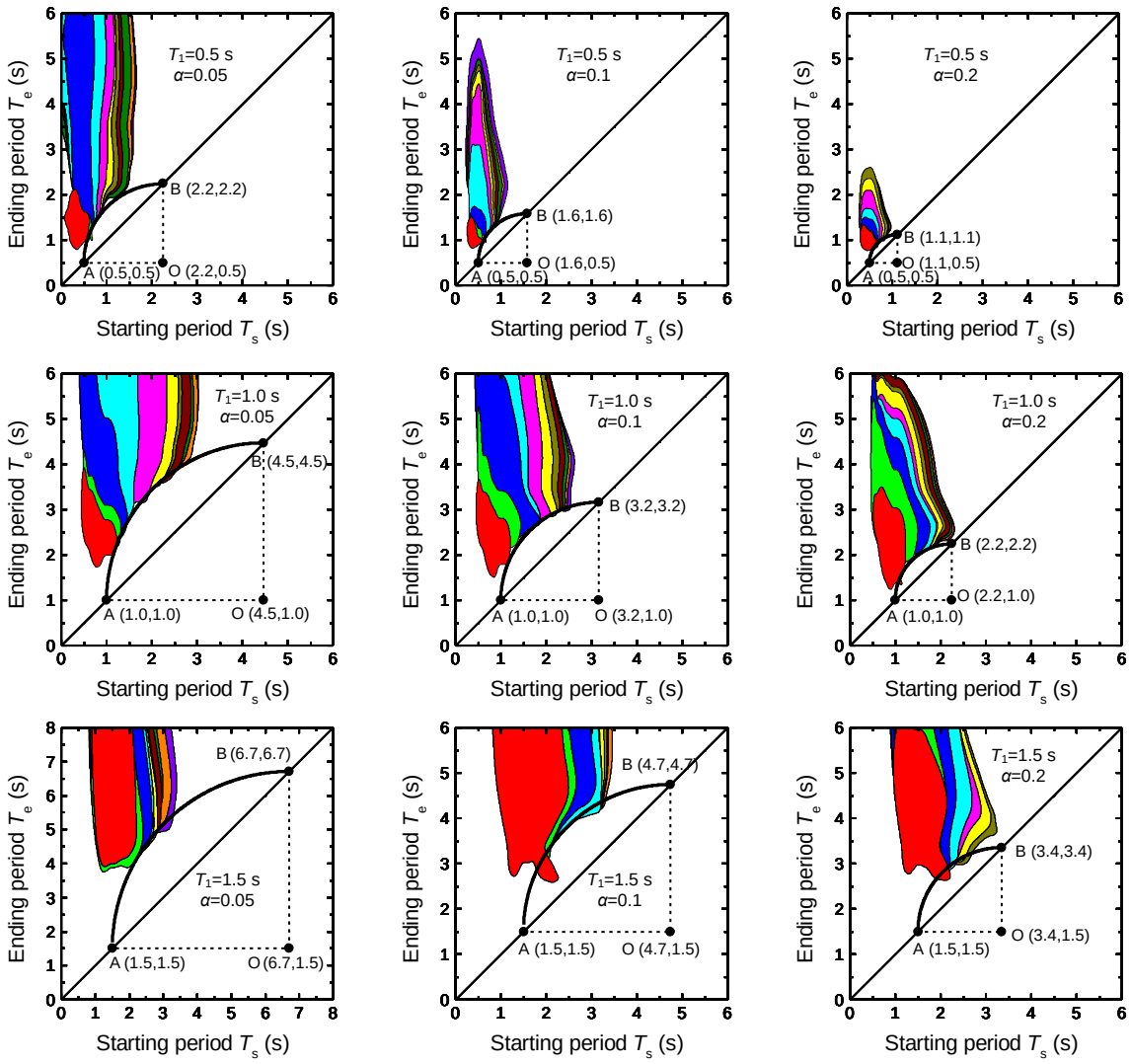


Fig. 14. Circle rule of SDOF bilinear systems with different structural parameters.

In the end, the proposed circle rule for constructing the DPI vector to achieve maximum damage correlation for a given bilinear system can be summarized mathematically as:

$$\begin{aligned} T_p &= \alpha^{-0.5} T_1 \\ T_s &= T_p - \left(T_p - T_1\right)\beta^{\lambda-1} \\ \left(T_s - T_p\right)^2 + \left(T_e - T_1\right)^2 &= \left(T_p - T_1\right)^2 \quad T_1 \le T_s, T_e \le T_p \end{aligned} \tag{27}$$

According to the above summarized equation, all the parameters needed in the vector-valued DPI can be calculated for a given bilinear system under a ground motion, in which the value of $\beta$ can be determined by the linear superposition using the Fig.15. If one wants to synthetize a ground motion which generates the same response for the given system under a natural record, the parameter $p_1$ and $p_2$ in the vector-valued DPI can be the criteria for the synthetizing ground motion in terms of response spectrum matching.

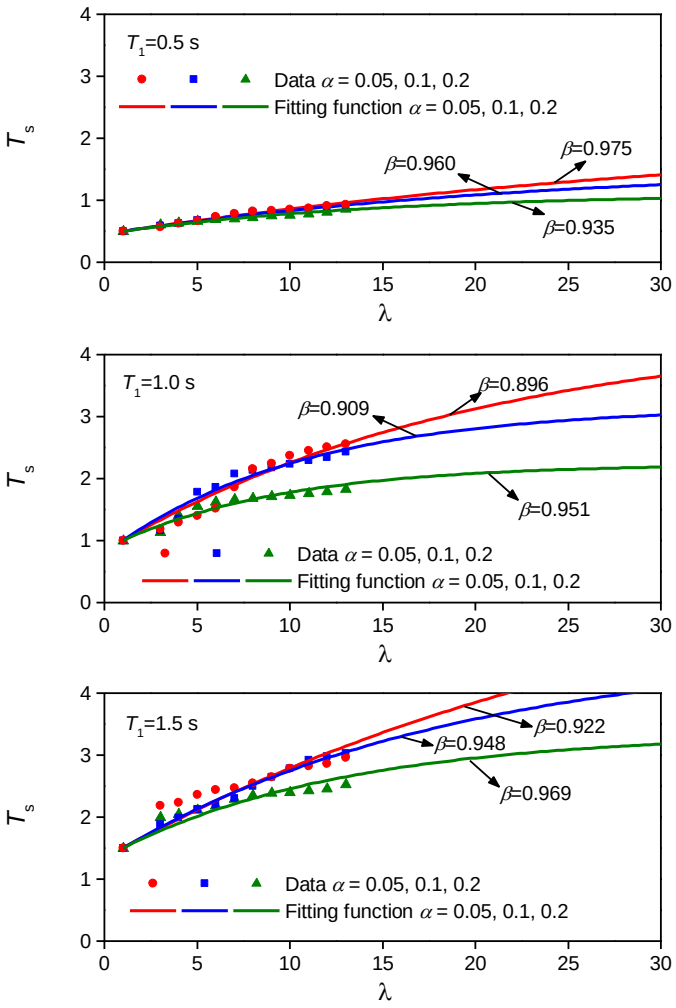


Fig. 15. Relationship between $\lambda$ and optimal starting period.

### 4.5. Potential application to BSI and validation

The proposed circle rule was calibrated using the 102 GM suite and seems to work quite well with bilinear system damage. The research team applied this rule to improve the efficiency of the existing BSI procedure and conducted validations with a limited number of simulations.

BSI is a procedure (Rezaeian et al. 2016; Sun et al. 2015) to improve synthetic GM models with the help of known recorded GMs. It is an iterative broadband synthetic GM generation program in which the user can apply different matching criteria or constrains to the synthetic GM spectrum against the recorded GM spectrum. If the user would like to have synthetic models that mimic the damage potential of a recorded earthquake, the circle rule can be applied to construct the matching constraints. The existing alternatives of BSI matching criteria are quite arbitrary. Sometimes the entire spectrum was matched in an average sense; sometimes only a few selected points on the spectrum were matched.

According to this circle rule, if the intensity of the recorded GM is given, and the structural parameters of the bilinear system are known, the target matching period range for BSI can be calculated. Then the BSI can be carried on to first match the spectral amplitude parameter and then the shape parameter in the target period range. As an example, a bilinear system with $T_1$=0.5s, $\alpha$=0.1, and $\xi$=5% was used in this study. Table 2 listed the spectrum matching constraints calculated based on the circle rule for 22 records from 11 Northridge stations (Group R). Note that this particular bilinear system was selected so that all these 22 GMs will induce damage on the system.

Table 2 spectral accelerations and period bands needed to be synthetized for 22 records

| Station/component | $S_a$(0.5s) (g) | $T_s$ (s) | $T_e$ (s) |
|---|---|---|---|
| cpp-106 | 0.931 | 0.65 | 1.05 |
| cpp-196 | 0.738 | 0.61 | 0.98 |
| hol-270 | 0.788 | 0.62 | 1.00 |
| hol-000 | 0.704 | 0.61 | 0.97 |
| jem-292 | 1.416 | 0.74 | 1.18 |
| jem-022 | 0.680 | 0.60 | 0.96 |
| jfp-292 | 1.298 | 0.72 | 1.15 |
| jfp-022 | 0.677 | 0.60 | 0.95 |
| nwp-000 | 1.645 | 0.78 | 1.22 |
| nwp-090 | 1.201 | 0.70 | 1.13 |
| par-000 | 0.876 | 0.64 | 1.03 |
| par-090 | 0.767 | 0.62 | 0.99 |
| rrs-228 | 1.775 | 0.80 | 1.24 |
| rrs-318 | 1.046 | 0.67 | 1.08 |
| sfp-000 | 0.515 | 0.57 | 0.88 |
| sfp-090 | 0.616 | 0.59 | 0.93 |
| syf-000 | 1.963 | 0.83 | 1.27 |
| syf-090 | 1.340 | 0.72 | 1.16 |
| van-270 | 1.446 | 0.74 | 1.18 |
| van-000 | 1.563 | 0.76 | 1.21 |
| wc1-090 | 0.672 | 0.60 | 0.95 |
| wc1-180 | 1.378 | 0.73 | 1.17 |

With these constraints identified, two group of synthetic GMs were generated. The first group (termed Group S) was generated using BSI procedure constrained by the circle rule period ranges. So this group conformed to the circle rule from a spectrum stand point, which should translate to similar structural damage (quantified by ductility of the bilinear system). As one can see in Table 3, the group S matches the recorded GM in both the value $\lambda$ and $p_1$. The BSI process is quite effective as one can see from Fig.16, the Group S synthetic spectrum fits the recorded spectrum very well at the locations indicated by the circle rule. The second group (Group B) was constructed from the synthetic ground motions in an earlier BSI attempt without the information about the circle rule. The basic spectrum DPI vector components for Group B are also listed in Table 3. One can see Group B is not as good as Group S for a match of Group R, if the circle

rule matching criteria is used. All three sets of GMs were applied to the bilinear system and the resulted ductility values are also listed in Table 3. If the circle rule can help improve damage predictability of synthetic GMs through BSI, the resulted ductility difference between Group R and B will be greater (statistically) than Group S.

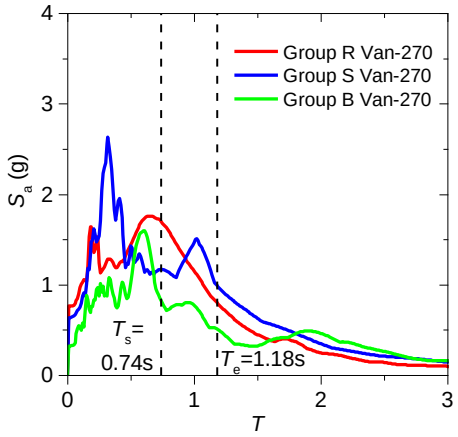


Fig. 16 Response spectra of Van-270 from Group R, Group S and Group B.

Table 3 Comparison between recorded and synthetic ground motions

| Station/component | Recorded Group R | | | Synthetic Group S | | | Synthetic Group B | | |
|---|---|---|---|---|---|---|---|---|---|
| | $p_2$ | $p_1$ | Ductility | $p_2$ | $p_1$ | Ductility | $p_2$ | $p_1$ | Ductility |
| cpp-106 | 4.66 | 0.537 | 2.64 | 4.66 | 0.54 | 3.32 | 4.27 | 0.788 | 3.3 |
| cpp-196 | 3.69 | 1 | 5.49 | 3.69 | 0.983 | 4.35 | 6.34 | 0.836 | 5.54 |
| hol-270 | 3.94 | 0.673 | 4.18 | 3.91 | 0.679 | 3.06 | 7.08 | 0.539 | 3.73 |
| hol-000 | 3.52 | 0.695 | 3.44 | 3.62 | 0.687 | 3.15 | 5.48 | 0.469 | 4.33 |
| jem-292 | 7.08 | 0.787 | 6.89 | 7.13 | 0.785 | 10.67 | 5.60 | 0.768 | 7.43 |
| jem-022 | 3.40 | 1.158 | 6.6 | 3.28 | 1.174 | 4.21 | 5.01 | 0.937 | 12.15 |
| jfp-292 | 6.49 | 1.285 | 6.92 | 6.46 | 1.294 | 8.42 | 6.15 | 0.599 | 6.81 |
| jfp-022 | 3.38 | 1.284 | 15.44 | 3.50 | 1.193 | 19.7 | 5.71 | 0.826 | 11.18 |
| nwp-000 | 8.23 | 0.748 | 12.69 | 8.18 | 0.757 | 15.74 | 2.89 | 1.015 | 10.76 |
| nwp-090 | 6.00 | 0.626 | 8.43 | 5.88 | 0.655 | 29.89 | 4.22 | 0.79 | 7.28 |
| par-000 | 4.38 | 1.676 | 14.87 | 4.29 | 1.723 | 18.52 | 3.42 | 1.574 | 7.57 |
| par-090 | 3.83 | 1.222 | 7.25 | 3.97 | 1.133 | 6.44 | 3.43 | 1.112 | 8.2 |
| rrs-228 | 8.88 | 1 | 28.41 | 8.87 | 0.996 | 19.88 | 5.12 | 0.59 | 5.08 |
| rrs-318 | 5.23 | 0.824 | 8.04 | 5.12 | 0.842 | 8.97 | 4.22 | 1.231 | 7.93 |
| sfp-000 | 2.58 | 1.044 | 2.33 | 2.58 | 1.045 | 3.34 | 4.42 | 1.229 | 5.94 |
| sfp-090 | 3.08 | 1.099 | 4.94 | 3.04 | 1.114 | 3.27 | 3.72 | 0.999 | 5.72 |
| syf-000 | 9.81 | 0.458 | 13.29 | 10.05 | 0.452 | 9.98 | 7.39 | 0.776 | 17.79 |
| syf-090 | 6.70 | 0.579 | 10.22 | 6.76 | 0.58 | 6.51 | 6.14 | 0.822 | 15.82 |
| van-270 | 7.23 | 0.857 | 16.21 | 7.13 | 0.869 | 12 | 5.10 | 0.693 | 6.02 |
| van-000 | 7.82 | 0.546 | 7.03 | 7.80 | 0.553 | 10.61 | 4.99 | 1.168 | 7.58 |
| wc1-090 | 3.36 | 0.657 | 2.41 | 3.45 | 0.66 | 2.82 | 4.65 | 0.713 | 4.98 |
| wc1-180 | 6.89 | 0.598 | 5.87 | 6.94 | 0.584 | 6.16 | 4.34 | 0.645 | 4.85 |

Fig. 17 shows that the comparison of ductility difference from Group R and S or Group R and B. One can also do a t-test on this ductility difference samples between the 2 cases. It was concluded that at 95% significance level, the means of these two groups are the same and the 2 cases are validated to be from a same distribution. Fig.18 shows the comparison of cumulative distribution function of the two cases. The almost overlapping curves also means that they have the same distribution feature.

We conclude that the circle rule does not improve the effectiveness of the ground motion synthetizing. One reason might be that the circle rule still has large scatter. The criteria of the period band identified is based on the coefficient of determination $R^2$, the large value of $R^2$ means the strong correlation between the similarity index and structural damages but not necessarily indicate a small dispersion. The other reason might be that the circle rule is proposed according to the 102 natural records and it is possibly not applicable for the synthetic ground motions.

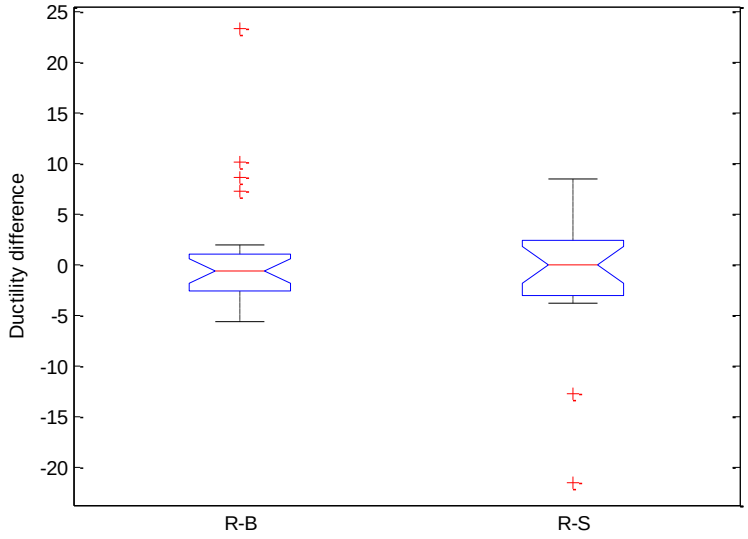


Fig. 17 Box plot of ductility differences of GroupR-GroupB and GroupR-GroupS.

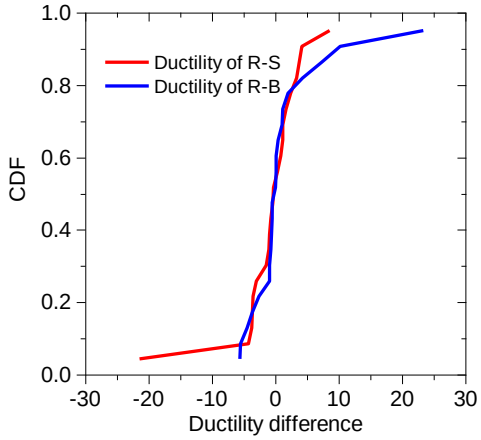


Fig. 18 CDF of ductility difference of R-S and R-B.

## 5. Conclusions

This research project started with an ambitious goal of developing a simple spectrum-based metric to calibrate synthetic GMs' damage potential to recorded GMs. The ability to do that will enable synthetic GM modelers to improve their model regarding structural damage

prediction using a tool (response spectrum) that they are very familiar with. The BSI procedure is believed to be a perfect way to combine this new matching guidance information with an existing broad-band synthetic GM model. Although it is well-known to the researchers that spectrum-matching will not yield a complete match for structural damage, this project seeks to advance our knowledge on the relationship between spectral shape and damage potential by identifying the key segment and characteristics of the response spectrum critical to the damage potential.

In this study, a DPI vector was formulated for the purpose of comparing the spectrum of different GMs. This DPI vector has an intensity component and a shape component. By applying a circle rule to this DPI vector, strong correlation between a generalized bilinear system damage and the DPI vector can be established.

The circle rule was applied to a BSI trial using limited number of ground motions. It was discovered that the advantage of introducing the circle rule in a BSI process does not significantly improve damage prediction accuracy. The potential reasons for this result are: 1) the circle rule is a sufficient but not necessary condition for achieving good damage correlation. Thus the BSI cases without applying the circle rule are not necessarily worse than the cases in which the circle rule was applied; 2) the number of GMs used for BSI validation was too limited to reflect the benefit of circle rule. Although the current attempt to apply the circle rule with BSI did not yield very satisfactory results, the efficiency of BSI can be used to improve constrains on matching without sacrificing damage predictability.

## 6. References


Akkar, S., and Özen, Ö. (2005). "Effect of peak ground velocity on deformation demands for SDOF systems." *Earthquake engineering & structural dynamics*, 34(13), 1551-1571.

Arias, A. (1970). "MEASURE OF EARTHQUAKE INTENSITY." Massachusetts Inst. of Tech., Cambridge. Univ. of Chile, Santiago de Chile.

Aydinoğlu, M. N. (2003). "An incremental response spectrum analysis procedure based on inelastic spectral displacements for multi-mode seismic performance evaluation." *Bulletin of Earthquake Engineering*, 1(1), 3-36.

Baker, J. W., and Allin Cornell, C. (2005). "A vector ‐ valued ground motion intensity measure consisting of spectral acceleration and epsilon." *Earthquake Engineering & Structural Dynamics*, 34(10), 1193-1217.

Baker, J. W., and Allin Cornell, C. (2006). "Spectral shape, epsilon and record selection." *Earthquake Engineering & Structural Dynamics*, 35(9), 1077-1095.

Bojorquez, E., and Iervolino, I. (2011). "Spectral shape proxies and nonlinear structural response." *Soil Dynamics and Earthquake Engineering*, 31(7), 996-1008.

Bradley, B. A., and Lee, D. S. (2010). "Accuracy of approximate methods of uncertainty propagation in seismic loss estimation." *Structural Safety*, 32(1), 13-24.

Calvi, G. M., Design, T. G. D. B., and Concrete, A. I. F. f. S. (2003). *Displacement-based seismic design of reinforced concrete buildings: state-of-art report*, Internat. Federation for Structural Concrete.

Cordova, P. P., Deierlein, G. G., Mehanny, S. S., and Cornell, C. A. "Development of a two-parameter seismic intensity measure and probabilistic assessment procedure." *Proc., The Second US-Japan Workshop on Performance-Based Earthquake Engineering Methodology for Reinforced Concrete Building Structures*, 187-206.

Deng, P., Pei, S., van de Lindt, J. W., and Zhang, C. (2017). "Uncertainty quantification for seismic responses of bilinear SDOF systems: A semi-closed-form estimation." *Soil Dynamics and Earthquake Engineering*, 93, 18-28.

Ellingwood, B. R., Celik, O. C., and Kinali, K. (2007). "Fragility assessment of building structural systems in Mid‐America." *Earthquake Engineering & Structural Dynamics*, 36(13), 1935-1952.

Ellingwood, B. R., and Kinali, K. (2009). "Quantifying and communicating uncertainty in seismic risk assessment." *Structural Safety*, 31(2), 179-187.

Fajfar, P., Vidic, T., and Fischinger, M. (1990). "A measure of earthquake motion capacity to damage medium-period structures." *Soil Dynamics and Earthquake Engineering*, 9(5), 236-242.

FEMA-P695 (2009). *Quantification of building seismic performance factors*, Federal Emergency Management Agency, Washington(DC).

Hartzell, S., Guatteri, M., Mai, P. M., Liu, P.-C., and Fisk, M. (2005). "Calculation of broadband time histories of ground motion, Part II: Kinematic and dynamic modeling using theoretical Green's functions and comparison with the 1994 Northridge earthquake." *Bulletin of the Seismological Society of America*, 95(2), 614-645.

Housner, G. "Measures of severity of earthquake ground shaking." *Proc., Proceedings of the US National Conference on Earthquake Engineering*, 25-33.

Iervolino, I., Manfredi, G., and Cosenza, E. (2006). "Ground motion duration effects on nonlinear seismic response." *Earthquake engineering & structural dynamics*, 35(1), 21-38.

Iwan, W. (1980). "Estimating inelastic response spectra from elastic spectra." *Earthquake Engineering & Structural Dynamics*, 8(4), 375-388.

Loth, C., and Baker, J. W. (2015). "Rational design spectra for structural reliability assessment using the response spectrum method." *Earthquake Spectra*, 31(4), 2007-2026.

Makris, N., and Black, C. J. (2004). "Evaluation of peak ground velocity as a "good" intensity measure for near-source ground motions." *Journal of Engineering Mechanics*, 130(9), 1032-1044.

Mazzoni, S., McKenna, F., Scott, M. H., and Fenves, G. L. (2006). "OpenSees command language manual." *Pacific Earthquake Engineering Research (PEER) Center*.

Medina, R. A., and Krawinkler, H. (2004). "Seismic demands for nondeteriorating frame structures and their dependence on ground motions." Pacific Earthquake Engineering Research Center.

Mehanny, S. S. (2009). "A broad-range power-law form scalar-based seismic intensity measure." *Engineering Structures*, 31(7), 1354-1368.

Park, Y. J., and Ang, A. H. S. (1985). "Mechanistic seismic damage model for reinforced concrete." *Journal of structural engineering*.

Park, Y. J., Ang, A. H. S., and Wen, Y. K. (1985). "Seismic damage analysis of reinforced concrete buildings." *Journal of Structural Engineering*.

Paulay, T., and Priestley, M. J. N. (1992). *Seismic Design of Reinforced Concrete and Masonry Buildings*, Wiley.

Rezaeian, S., Hartzell, S., Sun, X., and Mendoza, C. (2016). "Simulation of Earthquake Ground Motions in the Eastern United States Using Deterministic Physics‐Based and Site‐Based Stochastic Approaches." *Bulletin of the Seismological Society of America*, 107, 149-168.

Riddell, R. (2008). "Inelastic response spectrum: Early history." *Earthquake Engineering & Structural Dynamics*, 37(8), 1175-1183.

Riddell, R., and Garcia, J. E. (2001). "Hysteretic energy spectrum and damage control." *Earthquake Engineering & Structural Dynamics*, 30(12), 1791-1816.

Sun, X., Hartzell, S., and Rezaeian, S. (2015). "Ground‐motion simulation for the 23 August 2011, Mineral, Virginia, earthquake using physics‐based and stochastic broadband methods." *Bulletin of the Seismological Society of America*, 105, 2641-2661.

Vamvatsikos, D., and Cornell, C. A. (2002). "Incremental dynamic analysis." *Earthq Eng Struct Dyn*, 31(3), 491-514.

Vamvatsikos, D., and Cornell, C. A. (2005). "Developing efficient scalar and vector intensity measures for IDA capacity estimation by incorporating elastic spectral shape information." *Earthquake engineering & structural dynamics*, 34(13), 1573-1600.

Wen, Y., and Wu, C.-L. (2001). "Uniform hazard ground motions for mid-America cities." *Earthquake spectra*, 17(2), 359-384.

Yin, Y.-J., and Li, Y. (2010). "Seismic collapse risk of light-frame wood construction considering aleatoric and epistemic uncertainties." *Structural Safety*, 32(4), 250-261.